SCIENCE CHINA
Information Sciences

• **Supplementary File** •

A Qi Compatible Wireless Power Receiver with Integrated Full-Wave Synchronous Rectifier

Chubin WU, Zhang ZHANG*, Jianmin ZENG, Xin CHENG & Guangjun XIE

School of Electronics Science and Applied Physics, Hefei University of Technology, Hefei 230009, China

Appendix A Working Principles

When the AC1 signal is high, the MOSFETs MOS1 and MOS4 turn on, MOS2 and MOS3 turn off, and the current from the coil flows through MOS1 to the load and flows back from MOS4 to the coil, as shown in Figure A1(a).Conversely, when the AC2 signal is high, the MOSFETs MOS2 and MOS3 turn on, MOS1 and MOS4 turn off, and the current from the coil flows through MOS2 to the load and flows back from MOS3 to the coil, as shown in Figure A1(b).

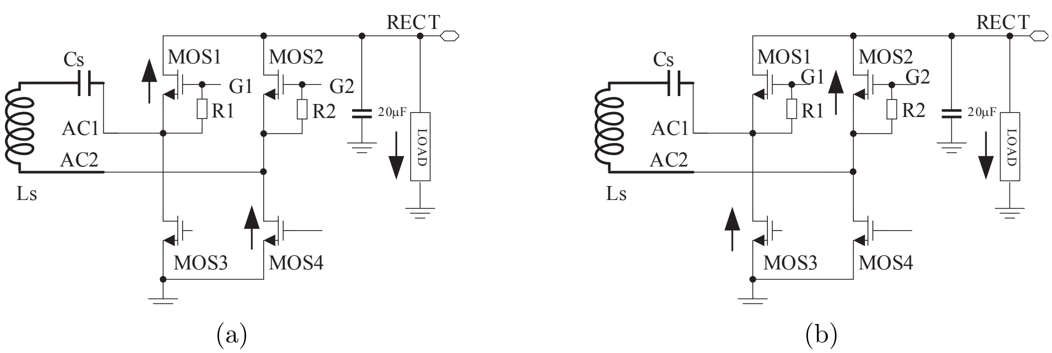

Figure A1 The illustration of the synchronous control of the MOSFETs

The resistors R1 and R2 shown in Figure A1 are used to speed up the setup time of the output of the drivers. For example, when AC1 changes from low to high, the gate voltage of MOS1 follows AC1 to change from low to high due to the existence of R1, and then the driver outputs a high pulse to turn MOS1 on. As Figure A2(a) shows, the output of the driver changes from AC1 to BOOT1. If there is no resistor between the source and the gate, the output of the driver must change from zero to BOOT1, as shown in Figure A2(b), which is much higher than that in Figure A2(a). Therefore, the resistors R1 and R2 can shorten the setup time of the drivers and improve the power efficiency of the rectifier. The resistances of R1 and R2 are chosen as 5Kconsidering the gate capacitance.

Figure A3 shows the block diagram of the proposed synchronous controller. The controller is used to generate the bidirectional non-overlapping clocks according to the polarity of the received AC input signal.

Figure A4 shows the timing diagram of the proposed digital pulse width controller. This controller uses the previous AC signal high-level width to generate a high pulse in the current AC cycle, and the high pulse is used to control the relevant high-side power MOSFETs to shut off before the AC signal changes from a high to low level. In this way, the turn-off delay could be eliminated effectively; therefore, the reverse leakage current is prevented, and the system efficiency can be improved.

Figure A5 illustrates the diagram of the non-overlapping clocks. The input signals are gotten from the output of the high-side voltage comparators, low-side voltage comparators, and the digital pulse width controller. The output signals are the non-overlapping clocks CLK_N1, CLK_N2, CLK_N3, and CLK_N4, which are used to control the relevant MOSFETs turn-on and turn-off to achieve a synchronous full wave rectifier. Figure A6 illustrates the timing diagram of the synchronous rectifier.

* Corresponding author (email: zhangzhang@hfut.edu.cn)

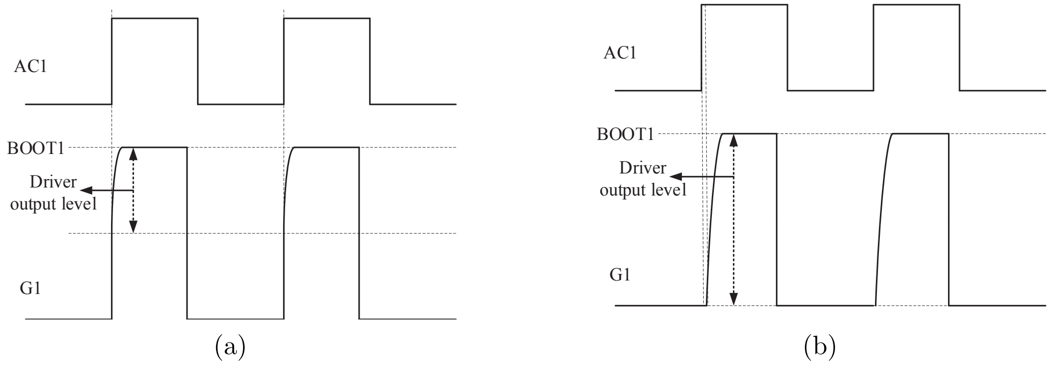

Figure A2 The timing diagram of the gate voltage (a) with resistor (b) without resistor

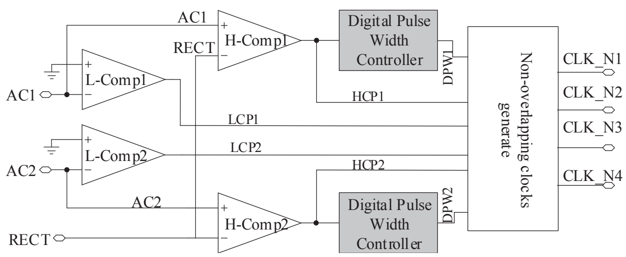

Figure A3 The block diagram of the proposed synchronous control logic module

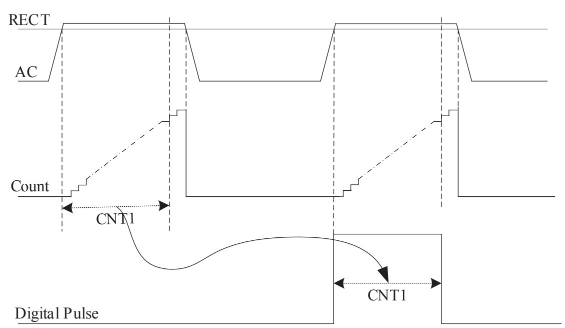

Figure A4 The timing diagram of the digital pulse width controller

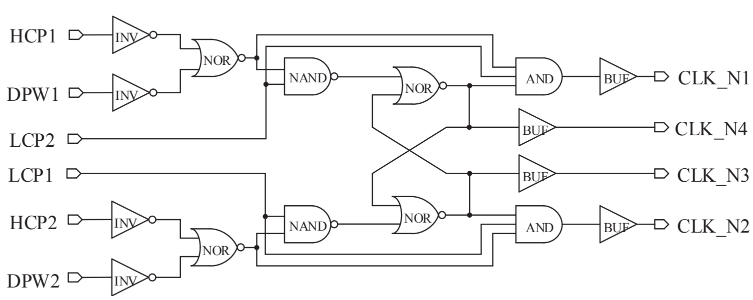

Figure A5 The diagram of the non-overlapping clocks generator

Appendix B Experimental results

Figure B1 shows the chip microphotograph, which occupied 9.9 mm^2.

Figure B2 illustrates the measurement environment of the wireless power transfer system. The transmitter (TX) coil and the receiver (RX) coil are located at the bottom and the top side, respectively. The power is transferred from the transmitter board to the receiver board through the TX coil and the RX coil.

Figure B3 shows the measurement results for the wireless power receiver. When the receiver is placed on a transmitter and the transmitter powers on, the RX coil receives the power from the TX coil. Then, the rectifier works in a passive

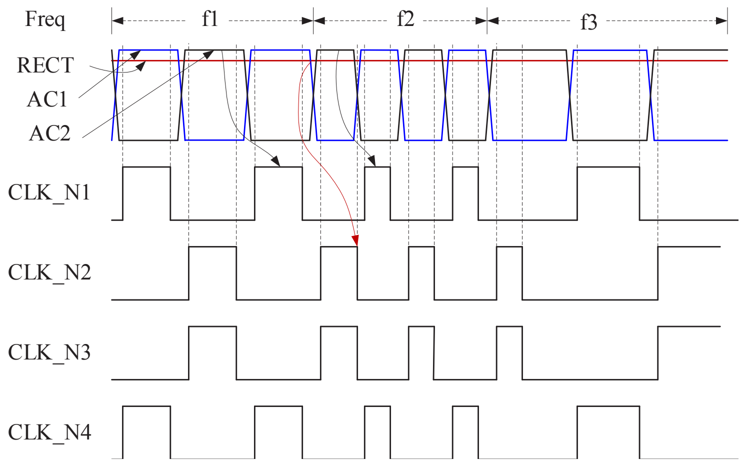

Figure A6 Timing diagram of the synchronous rectifier

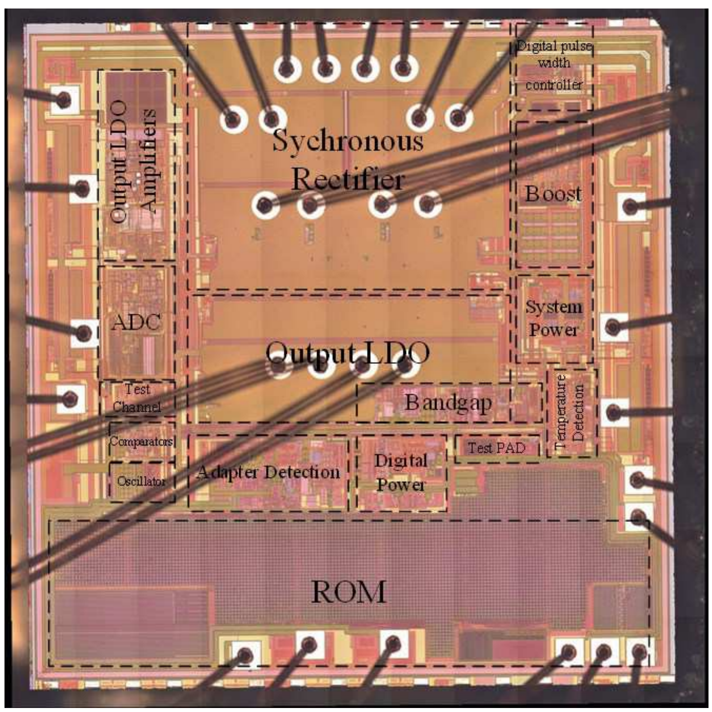

Figure B1 The chip microphotograph

Table B1 The main parameter of the system

Parameter	Transmitter	Receiver
Coil Inductance	7μH	11.2μH
Resonant Capacitance	400nF	204nF
Resonant Frequency	95KHz	106KHz
Vertical Dimension	4mm	4mm
Operation Frequency	110-205KHz	-
Vin	5V	-

diode mode to generate the RECT voltage, and the receiver starts working and communicating with the transmitter. When

Figure B2 Measure environments of the wireless power transfer system

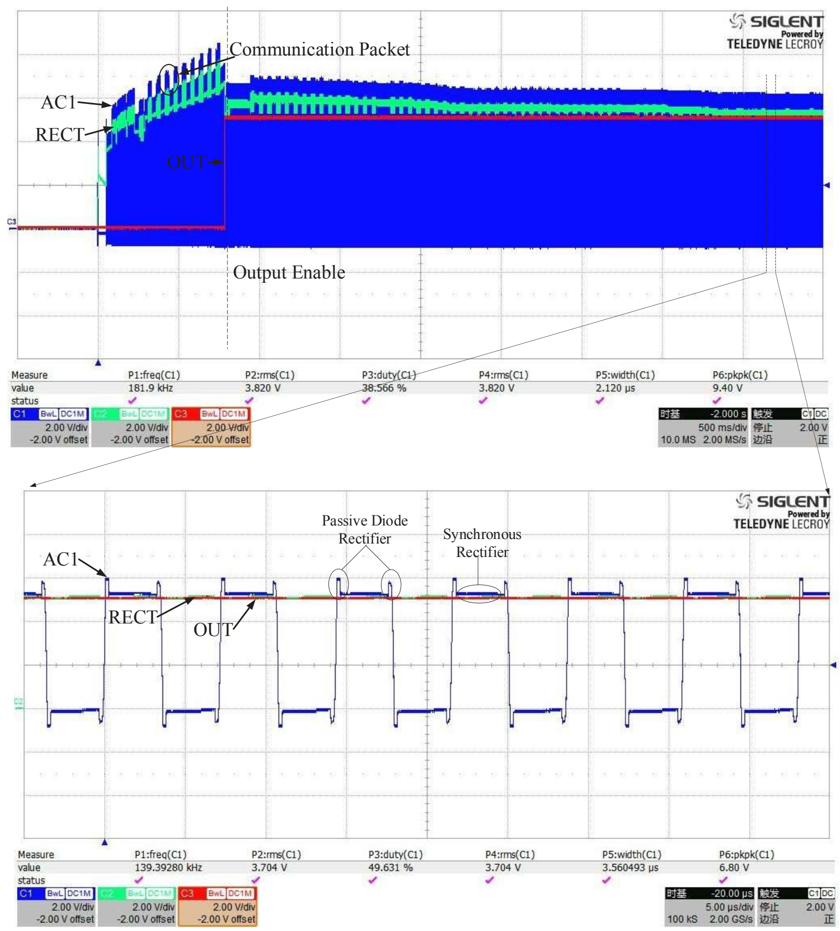

Figure B3 Measurement results of the wireless power receiver

the output condition is satisfied, the output is enabled, and the receiver continues to communicate with the transmitter to dynamically control the RECT voltage according to the output power. The output power shown in Figure B3 is 5W, and the RECT voltage is finally close to the output voltage of 5V. As shown in the large view of Figure B3, from the AC1 signal wave we see that the synchronous rectifier can effectively eliminate the turn-off delay of the MOSFETs.

Figure B4 shows the measured power efficiency of the wireless power system. Table B1 shows the main parameters of this system. The output current is swept from 0.1A to 1A, and the peak power efficiency of the system is 82% at the 0.9A output current. Table B2 summarizes the comparison between related wireless power receivers reported elsewhere and in this paper. The maximum output power and the system efficiency in [1] is lower than that of this work. It is illustrated in [2] that the same maximum output power as does this paper, while the system efficiency of the wireless power receiver proposed in this paper is higher than that of [2]. The maximum output power in [3-5] is much smaller than that of in this paper.

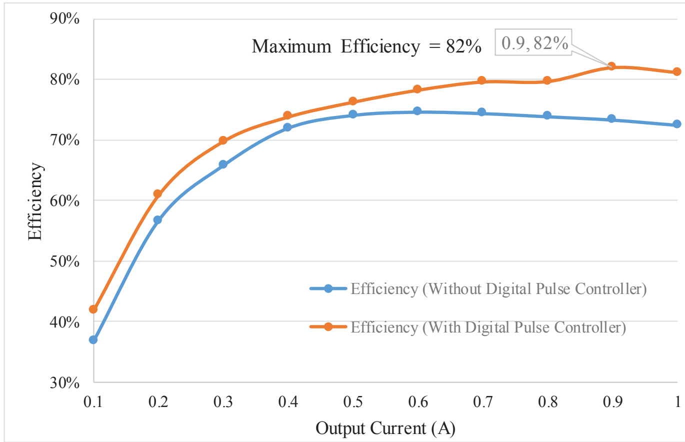

Figure B4 The measured power efficiency of the wireless power system

Table B2 Tabel Performance summary of the wireless power receiver system

Reference	[4]	[8]	[14]	[15]	[16]	This work
Technology	0.18µm BCD	N/A	0.18µm CMOS	0.18µm CMOS	0.18µm COMS	0.18µm BCD
Working Frequency (KHz)	100-300	100-200	100-150	13.56MHz	13.56MHz	110-205
System Efficiency (%)	63@2.5W	(68-72)@(2.5-5)W	82@peak	70-87	55@peak	82@0.9A
Maximun Coil Separation dc(MAX)	N/A	30mm	11mm	20mm	10mm	10mm
Lp	N/A	N/A	12.8mH	3.12 µH	N/A	11.2µH
CP	N/A	N/A	110pF	N/A	N/A	204nF
Ls(µH)	N/A	12.5	400	4.13	0.98	7
Cs	N/A	N/A	No Cs	33pF	141pF	400nF
Output Voltage (V)	3.5 to 5	5	1.2	2.3 to 3	1.8	5
Max Output Power (W)	2.5	5	224µW	632µW	12µW	5
Die Area (mm^2)	5.83	N/A	0.49	0.45	4.8	9.9

References

1 Hwang J T, Lee D S, Lee J H, et al. An All-in-One (Qi, PMA and A4WP) 2.5W Fully Integrated Wireless Battery Charger IC for Wearable Applications. In: Proceedings of the IEEE International Solid-State Circuits Conference, 2016. 378-380.

2 Riehl P S, et al. Wireless power systems for mobile devices supporting inductive and resonant operating modes. IEEE Transactions on Microwave Theory and Techniques, 2015, 63(3): 780790.

3 Lazaro O, Rincn-Mora G A. 180-nm CMOS Wideband Capacitor-Free Inductively Coupled Power Receiver and Charger. IEEE Journal of Solid-State Circuits, 2013, 48(11): 2839-2849.

4 Lee S-Y, Hong J-H, Hsieh C H, et al. A low-power 13.56 MHz RF front-end circuit for implantable biomedical devices. IEEE Transactions on Biomedical Circuits and Systems, 2013, 7(3): 256265.

5 Yoo J, Yan L, Lee S, et al. A 5.2 mW self-configured wearable body sensor network controller and a 12W wirelessly powered sensor for a continuous health monitoring system. IEEE Journal of Solid-State Circuits, 2010, 45(1): 178188.